INTERNATIONAL JOURNAL FOR NUMERICAL METHODS IN FLUIDS
Int. J. Numer. Meth. Fluids 2002; **40**:697–721 (DOI: 10.1002/fld.370)

A numerical study of the behaviour of a gas–liquid interface subjected to periodic vertical motion

J. Valha[1], J. S. Lewis[2] and J. Kubie[3,*,†]

[1] *Westinghouse* (*Process Control Europe*), *120 00 Prague 2*, *Czech Republic*
[2] *School of Engineering Systems*, *Middlesex University*, *London N11 2NQ*, *England*
[3] *School of Engineering*, *Napier University*, *Edinburgh EH10 5DT*, *Scotland*

SUMMARY

A numerical study has been undertaken to examine the behaviour of a gas liquid interface in a vertical cylindrical vessel subjected to a sinusoidal vertical motion. The computational method used is based on the simplified marker-and-cell method and includes a continuum surface model for the incorporation of surface tension. The numerical results indicate that the surface tension has very little effect on the period and amplitude of oscillations of the interfacial waves. The stability of the interfacial waves has been found to depend on the initial pressure pulse disturbance, and exponential growth of the interfacial wave has been observed in some cases. The influence of the amplitude and frequency of the forcing oscillations has also been investigated. The results are in good agreement with available experimental and analytical solutions. Copyright © 2002 John Wiley & Sons, Ltd.

KEY WORDS: numerical study; gas–liquid; interface; periodic motion

1. INTRODUCTION

Surface waves generated by vertically vibrating a horizontal fluid layer have been studied for a long time. Faraday [1] was possibly the first investigator to conduct systematic experiments and observed surface waves on ink, water, alcohol, milk and other liquids. He noted the important property that the frequency of the waves was half the frequency of the forcing vibration. Later Rayleigh [2] suggested a theoretical treatment of the problem, supported by more detailed observations. In general, the investigation of horizontal fluid layers subjected to vertical oscillation is known as the determination of Faraday stability.

Surface waves induced by vertical motion have recently received renewed attention, as the principles of wave instability are important in many areas, such as spray technologies and ink jet printers. A more comprehensive overview is given by Valha and Kubie [3].

This article is based on the work of Valha [4], who investigated the stability of gas–liquid interfaces in a vertical cylindrical vessel subjected to a sinusoidal vertical motion. The paper

* Correspondence to: J. Kubie, School of Engineering, Napier University, Edinburgh EHIO 5DT, Scotland.
† E-mail: j.kubie@napier.ac.uk

Received January 2001
Revised January 2002

by Valha and Kubie [3] described the experimental work, which indicated that there was a certain limiting critical frequency at which the gas–liquid interface became unstable, significant amounts of liquid were thrown vertically upwards from the interface and the interface thus lost its coherent structure. The experimental results were compared with an analytical solution based on the reduction of governing non-viscous equations to a Mathieu equation, and good agreement between theory and experiment was found.

It is the purpose of this paper to describe a computational fluid dynamics (CFD) approach to the solution of a more general problem, which, in contrast to the previous work, additionally considers the effect of the liquid viscosity. Typical numerical results are presented and compared with the previously obtained analytical results for inviscid flow.

2. COMPUTATIONAL WORK

2.1. Governing equations

Following the work of Valha and Kubie [3], we consider a cylindrical column of radius R (diameter D) and height L, as shown in Figure 1. This cylinder, containing a liquid layer of height l in its bottom section and air in its top section, and closed at both ends, is subjected to regular sinusoidal oscillatory motion along its vertical axis with the upward acceleration a is given by

$$a = A\omega^2 \cos(\omega t) \tag{1}$$

By physical equivalence we can regard the system as a stationary column subjected to oscillatory acceleration in the vertical direction given by

$$g_z = -g - A\omega^2 \cos(\omega t) \tag{2}$$

The basic equations describing two-dimensional, time-dependent flow of a constant viscosity incompressible fluid are

$$D \equiv \frac{1}{r^\alpha}\frac{\partial r^\alpha u}{\partial r} + \frac{\partial v}{\partial z} = 0 \tag{3}$$

$$\frac{\partial u}{\partial t} + \frac{1}{r^\alpha}\frac{\partial r^\alpha u^2}{\partial r} + \frac{\partial uv}{\partial z} = -\frac{\partial \Phi}{\partial r} + g_r + v\frac{\partial}{\partial z}\left(\frac{\partial u}{\partial z} - \frac{\partial v}{\partial r}\right) + F_{br} \tag{4}$$

$$\frac{\partial u}{\partial t} + \frac{1}{r^\alpha}\frac{\partial r^\alpha uv}{\partial r} + \frac{\partial v^2}{\partial z} = -\frac{\partial \Phi}{\partial z} + g_z - \frac{v}{r^\alpha}\frac{\partial}{\partial r}\left[r^\alpha\left(\frac{\partial u}{\partial z} - \frac{\partial v}{\partial r}\right)\right] + F_{bz} \tag{5}$$

where F_{br} and F_{bz} represent the forces due to surface tension and their significance, as well as the method of computation, is discussed later. Equation (3) represents continuity, and Equations (4) and (5) describe conservation of momentum in the r and z directions, respectively. When working in Cartesian co-ordinates $\alpha = 0$ and when in cylindrical co-ordinates $\alpha = 1$. Furthermore, for the vertically vibrating system analysed in this work, the horizontal component of acceleration in Equation (4) is $g_r = 0$.

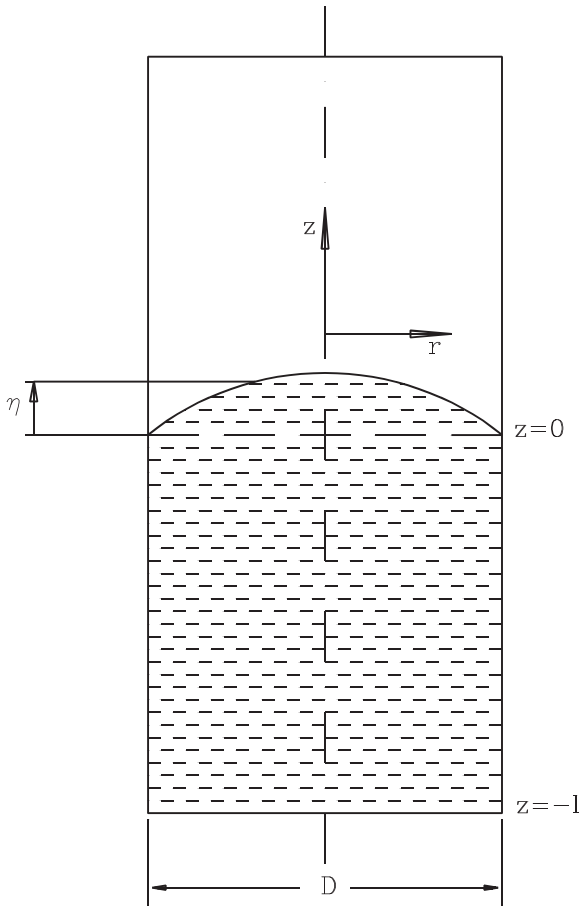

Figure 1. Diagram of the system investigated in the present work.

2.2. Computational method

2.2.1. General considerations. A number of methods are available for the simulation of problems concerning time-dependent viscous flow of incompressible fluid in several space dimensions. The most widely used method is probably the marker-and-cell (MAC) method developed by Welch *et al.* [5]. This method explicitly discretizes the time-dependent governing equations and utilizes a grid of massless Lagrangian particles that are used for the representation of the position of the fluid. The rearrangement of the equations then yields a Poisson equation for pressure. A further development of the technique, the simplified marker-and-cell (SMAC) method of Amsden and Harlow [6] simplifies the problem. In the SMAC method the pressure is not calculated over the whole computational domain, but only at the free surface and hence the problems associated with the solution of the Poisson equation for pressure, when solving Equations (3)–(5) are avoided. The SMAC method was used in the present analysis.

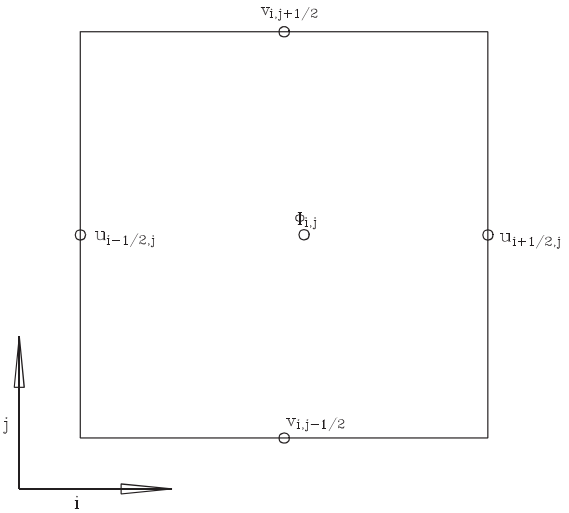

Figure 2. SMAC computational mesh.

The essence of the computational procedure is as follows. Vorticity Ω, given by

$$\Omega = \frac{\partial u}{\partial z} - \frac{\partial v}{\partial r} \tag{6}$$

is independent of pressure. Hence, any field of pressure inserted into Equations (4) and (5) will ensure that the resulting velocity field carries consistent vorticity.

Equations (3)–(6) are re-written in explicit finite difference form. The true pressure, normalized to unity density, Φ is replaced by an arbitrary pressure field θ. The notation associated with a typical SMAC finite difference cell is shown in Figure 2. The finite difference forms of the r-direction and the z-direction momentum conservation equations (4) and (5) are then combined to obtain a transport expression for the vorticity Ω which is independent of the pressure field θ. The boundary conditions for the walls and the free surface are then specified in the usual way. The explicit calculation of the initial velocities then ensures that the vorticity at every mesh point is consistent and independent of the choice of θ. In the second phase of the calculations the initial velocity field is adjusted into the final velocity field that satisfies continuity for every cell.

In addition to the mesh of Eulerian cells, shown in Figure 2, the SMAC algorithm employs a set of massless marker particles, which enable visual representation of the fluid, but whose essential purpose is to define the position of the free surface so that the configuration of the surface cells can be determined.

2.2.2. Modelling of surface tension. The influence of surface tension is given in Equations (4) and (5). In the present analysis the surface tension phenomena are modelled using the continuum surface force (CSF) model of Kothe *et al.* [7]. The model interprets surface tension as a continuous multidimensional effect across an interface, rather than a boundary value condition on the interface as used by Welch *et al.* [5]. As mentioned above, the effect is modelled via the F_{br} and F_{bz} terms in Equations (4) and (5), respectively.

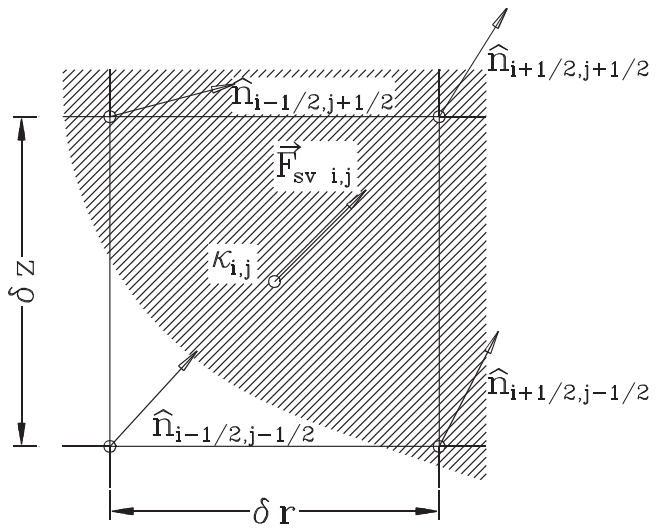

Figure 3. Notation used for the evaluation of the effects of surface tension.

The volume force due to surface tension is given as

$$\vec{F}_{sv}(\vec{x}) = \sigma\kappa(\vec{x})\nabla F(\vec{x}) \tag{7}$$

where, as discussed by Hirt and Nichols [8], the volume of fluid (VOF) function F represents the fractional volume of the cell occupied by the fluid. Cells with the F values between zero and one contain a free surface. Hirt and Nichols [8] devised an algorithm for accurate solution of the differential equation for the transport of F. The method used in this work to obtain the values of F on the surface was to split the surface cells using a subgrid.

The surface curvature κ is given by Drazin and Reid [9] as

$$\kappa = -(\nabla \cdot \hat{n}) = \frac{1}{|\vec{n}|} \cdot \left[\left(\frac{\vec{n}}{|\vec{n}|} \cdot \nabla \right) |\vec{n}| - (\nabla \cdot \vec{n}) \right] \tag{8}$$

where the unit normal

$$\hat{n} = \frac{\vec{n}}{|\vec{n}|} \tag{9}$$

is derived from the normal vector given by the gradient of the F function

$$\vec{n} = \nabla F(\vec{x}) \tag{10}$$

The volume force F_{sv} given by Equation (7) is located at the computational cell centres. Equation (7) shows that the curvature κ must also be located at the cell centres. The CSF model for the surface tension applied in the present analysis places the normal vector at the vertices, taking the cell centred normal as the average of the vertex normals, and the curvature κ at the cell centres, as shown in Figure 3. The details of the finite difference expansion of

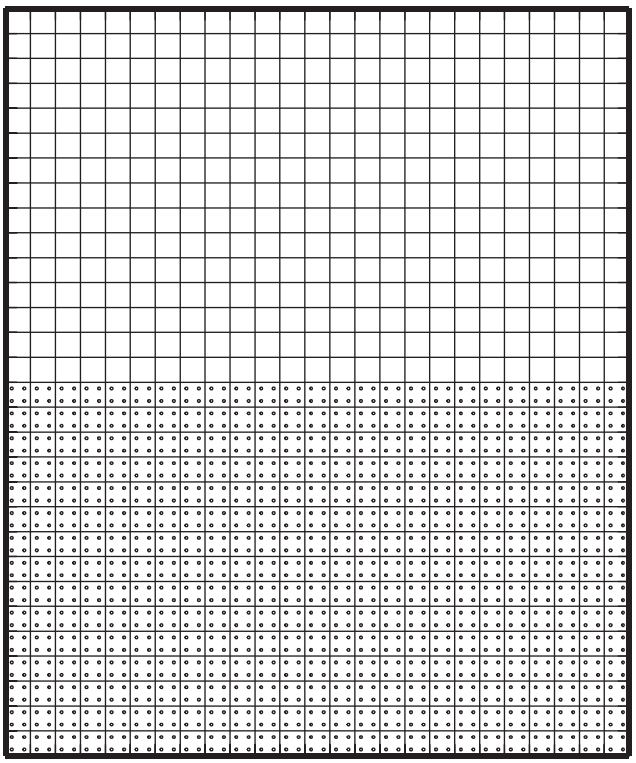

Figure 4. Computational mesh used for the numerical experiments.

Equations (7)–(10) are given, for example, by Brackbill *et al.* [10] and are not presented here.

The components of F_{sv} in the r and z directions are obtained by evaluating the r and z components of the mesh corner normals, as shown in Figure 3, and then taking their average to get the cell centred value; hence

$$F_{sv\,r} \equiv |\vec{F}_{sv\,r}(\vec{x})| = \sigma\kappa\vec{n}_r \tag{11}$$

$$F_{sv\,z} \equiv |\vec{F}_{sv\,z}(\vec{x})| = \sigma\kappa\vec{n}_z \tag{12}$$

Finally, the components of the surface tension force in Equations (4) and (5) are normalized by the fluid density, so that

$$F_{br} = \frac{F_{sv\,r}}{\rho} \tag{13}$$

$$F_{bz} = \frac{F_{sv\,z}}{\rho} \tag{14}$$

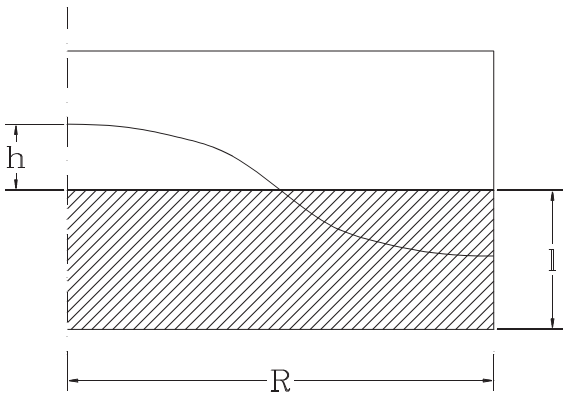

Figure 5. Diagram of the pressure pulse wave applied on the free surface.

are the source terms representing the effects of surface tension in the computational procedure; these terms are, as indicated by Equations (4) and (5), additional to the accelerations g_r and g_z in each cell.

2.2.3. Overview of the computational cycle. The equations presented above, rewritten in finite difference form, have been implemented in a computer program for calculation of the time-dependent fluid velocity components and the corresponding marker particle positions. To simplify the handling of boundary conditions, the program also employs a single layer of boundary cells on all four sides of the mesh. The problem specific input data includes the values of the fluid properties ρ, ν and σ, details of the domain boundary conditions (either free-slip or no-slip), the frequency and amplitude of the vertical sinusoidal forcing oscillations and the shape of the pressure pulse initially applied to the free surface. In addition, information is required on the number of marker particles as well as their initial distribution and initial velocity components. Cell flags are then initialized to indicate boundary wall cells, empty cells, full cells, and free surface cells. Values must also be given for the over-relaxation parameter used in an iterative calculation performed at each time step and the associated convergence tolerance to be satisfied. Apart from the addition of surface tension modelling the computational cycle follows the SMAC methodology described in detail by Amsden and Harlow [6].

The remainder of the computational cycle comprises three phases. In the first phase a tentative set of new-time velocities, referred to as tilde velocities, is calculated using an arbitrary pressure distribution θ. As a first step, values of $\theta_{i,j}$ are generated for each cell. For full cells $\theta_{i,j}$ is arbitrarily set to zero. However, in the surface cells, $\theta_{i,j}$ is taken to include the applied pressure Φ(applied) on the free surface, the surface tension stress and the viscous contribution to the normal stress. Next, boundary conditions are invoked to determine appropriate tangential velocity values for the cells just outside the surface cells and the boundary cells, that satisfy the free surface tangential stress condition and free-slip or no-slip wall condition, respectively. The tilde velocities are then calculated from Equations (4) and (5), written in explicit finite difference form, with the terms $F_{\mathrm{b}r}$ and $F_{\mathrm{b}z}$ representing the influence of surface tension evaluated as described in Section 2.2.2. Velocities at the empty-cell faces of surface

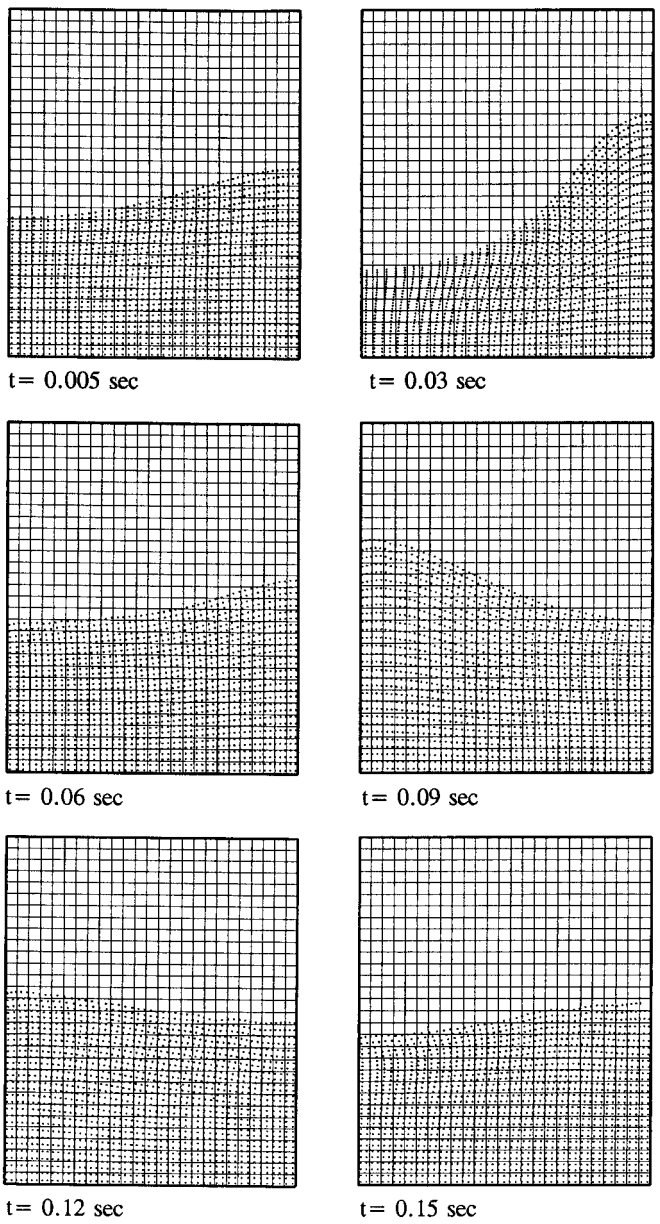

Figure 6. Time sequence of the interfacial position of glycerol ($\sigma = 0.00\ \mathrm{N\ m^{-1}}$, $A = 70$ mm, $f = 3$ Hz, $h = 20$ mm).

cells are not, however, evaluated at this stage (see below). The correct specification of velocity boundary conditions ensures that the resulting tilde velocity field carries the correct vorticity, regardless of the arbitrary nature of the pressure distribution assumed. However, this tentative set of velocities does not satisfy the continuity Equation (3).

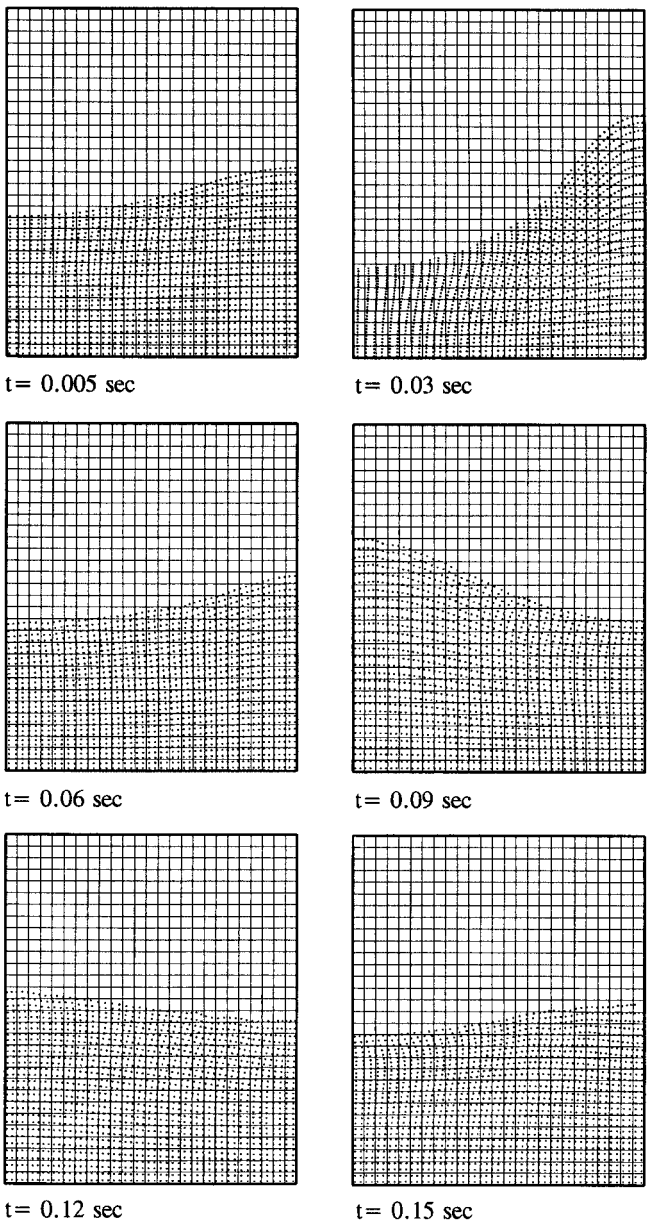

Figure 7. Time sequence of the interfacial position of glycerol ($\sigma = 0.03$ N m^{-1}, $A = 70$ mm, $f = 3$ Hz, $h = 20$ mm).

The purpose of the second phase is to adjust the tilde velocities in such a manner that the final velocity field preserves the vorticity embedded during the first phase of the calculation, and also satisfies the continuity Equation (3) in finite difference form for every cell, i.e. $D_{i,j} = 0$. As a first step, the tilde velocities are used to calculate values of this divergence

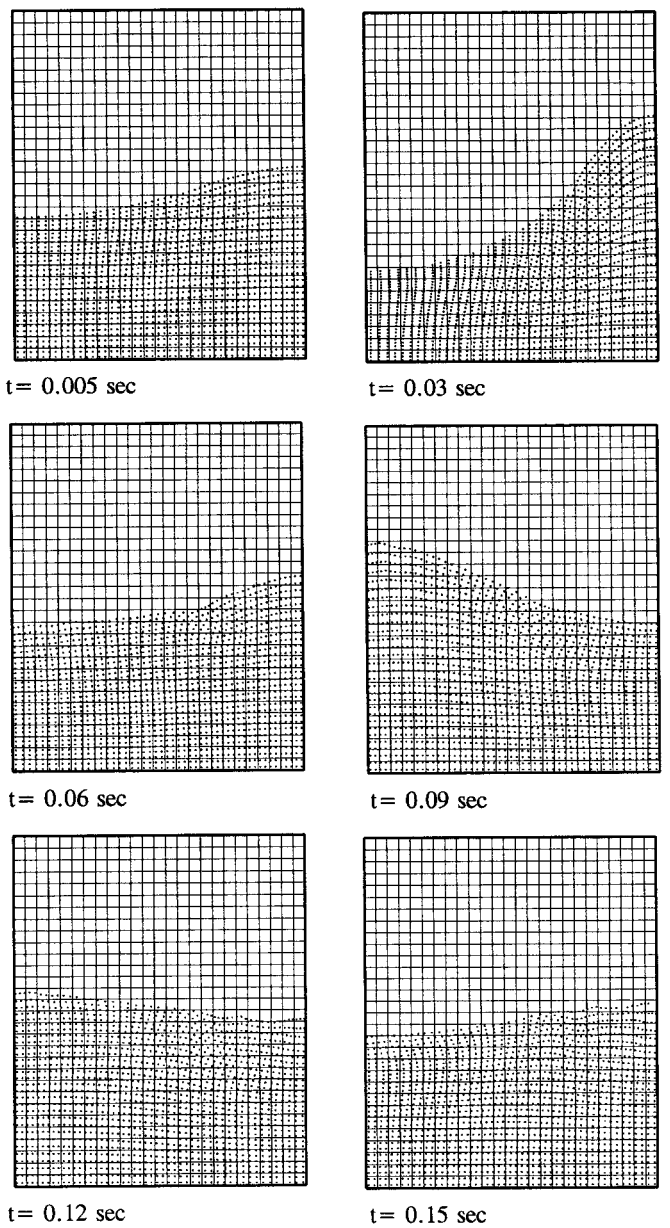

Figure 8. Time sequence of the interfacial position of glycerol ($\sigma = 0.15\ \mathrm{N\ m^{-1}}$, $A = 70$ mm, $f = 3$ Hz, $h = 20$ mm).

which consequently do not vanish as required. The necessary adjustment of the velocity field is equal to the local gradient of the potential function. Values of this function are calculated for the full cells only by an iterative finite difference solution of the governing equation, derived from Equation (3), using a point-by-point successive over-relaxation scheme. For

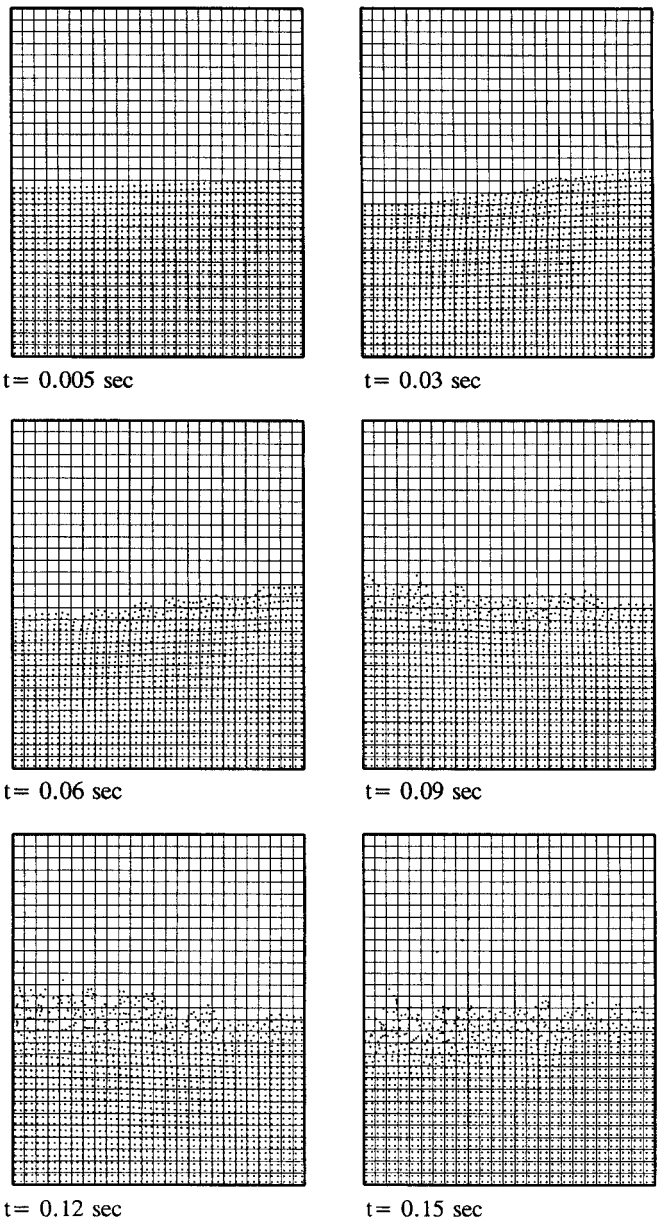

Figure 9. Time sequence of the interfacial position of water ($\sigma = 0.00\ \mathrm{N\ m^{-1}}$, $A = 70$ mm, $f = 2$ Hz, $h = 2.5$ mm).

the surface cells, the function is set to zero. The procedure just described is applied to evaluate the final corrected velocities at all cell faces other than the empty-cell faces of surface cells, where the normal velocities are determined by enforcing that $D_{i,j} = 0$ for each surface cell. As a final step in this phase, the tangential velocities in the cells just outside

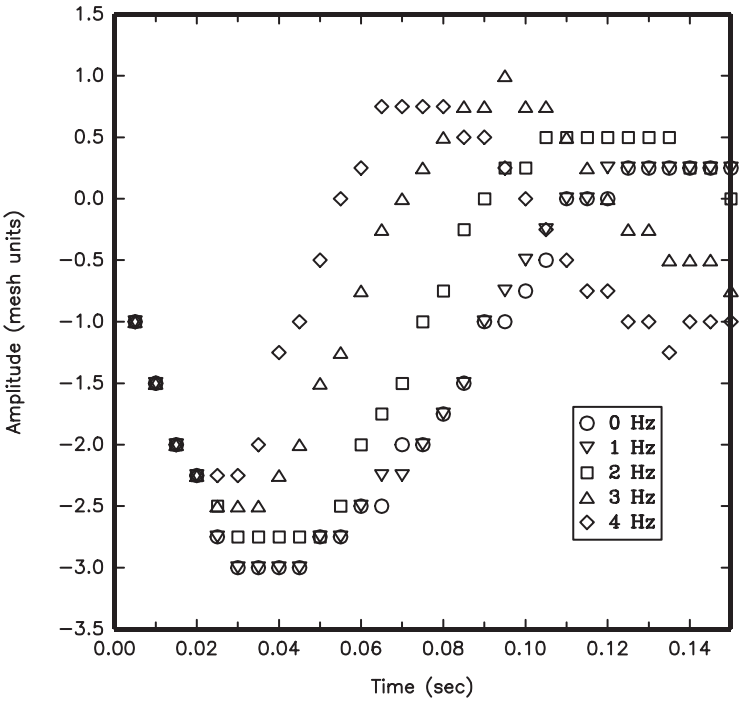

Figure 10. A plot of the wave displacement of glycerol at the axis of symmetry as a function of time ($\sigma = 0.00\ \mathrm{N\,m^{-1}}$, $A = 70\ \mathrm{mm}$, $h = 5\ \mathrm{mm}$).

the surface cells and the boundary cells are reset by the same procedure as used in the first phase.

In the third phase the new marker particle co-ordinates, in the r and z directions, are calculated based on area-weighted averages of the four nearest values of the corrected velocities u and v. Finally, control is returned to the reflagging section to begin the next time cycle.

3. RESULTS AND DISCUSSION

The numerical method described in the above section has been applied to investigate the behaviour of interfacial surface waves induced by vertical sinusoidal motion. A number of numerical experiments were carried out to investigate the influence of the liquid properties, the nature of the forcing oscillations and the initial disturbance on the interfacial surface.

All numerical experiments were run on a two-dimensional 25×30 uniform cylindrical co-ordinate mesh of 0.00138 m grid size in both the r and z directions, corresponding to the size of the 69 mm diameter cylinder used in the experimental work described by Valha and Kubie [3]. The mesh shown in Figure 4 represents only half of the cylinder as the problem is axially symmetrical. The axis of symmetry is located on the left-hand boundary of the computational mesh. All boundaries were chosen to be of free-slip type, thus exerting no drag upon the fluid.

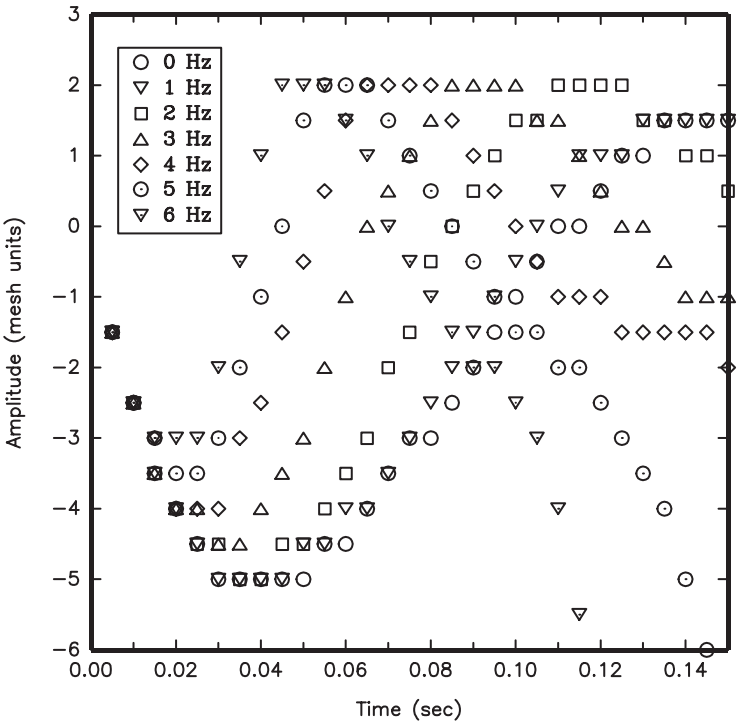

Figure 11. A plot of the wave displacement of glycerol at the axis of symmetry as a function of time ($\sigma = 0.00\ \mathrm{N\,m^{-1}}$, $A = 70\ \mathrm{mm}$, $h = 10\ \mathrm{mm}$).

Four marker particles per cell, initially uniformly distributed, were used throughout the present numerical work. Figure 4 shows the initial distribution of the liquid inside the computational domain. The previous work of Valha and Kubie [3] indicates that the influence of the liquid height on the behaviour of the interfacial wave is expressed via a $\tanh(k_m l)$ term. If only the first and second modes of oscillation are assumed to occur on the interface, the $\tanh(k_m l)$ values are 0.894 and 0.997, respectively. These values are sufficiently close to 1, and therefore the effects of the liquid base, represented by the lowest part of the computational domain, on the numerical result may be neglected. The typical timestep used was 0.0001 s. Tests were also run with a halved timestep and halved mesh size but no significant changes in results obtained were found.

The calculations were started by applying a pressure pulse in the form of a sinusoidal wave on the surface cells for the first time cycle. This form was chosen because it approximates the shape of the surface observed during the experimental work of Valha and Kubie [3]. It should be noted that in the surface cells, the pseudopressure is equal to the true pressure. The term representing the pulse, which is added to the surface pressure Φ, and denoted by $\Phi(\mathrm{applied})$ is given by

$$\Phi(\mathrm{applied}) = \frac{B\cos(XCr)}{\delta t} \tag{15}$$

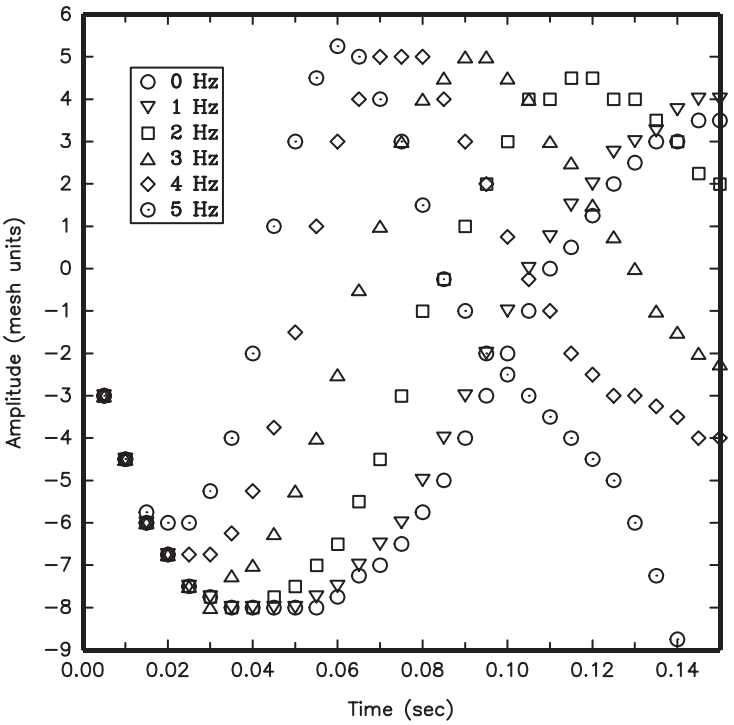

Figure 12. A plot of the wave displacement of glycerol at the axis of symmetry as a function of time ($\sigma = 0.00\ \mathrm{N\ m^{-1}}$, $A = 70\ \mathrm{mm}$, $h = 20\ \mathrm{mm}$).

where X is a parameter equal to 1 for a half sinusoidal wave and 2 for a full sinusoidal wave. Only the two cases of $X = 1$ and 2 were investigated in the present work. Parameters B and C, obtained as a result of linear analysis for a rectangular vessel [9], are defined with reference in Figure 5 as

$$B = h\sqrt{\frac{gl}{\xi}} \tag{16}$$

$$C = \frac{\pi}{R} \tag{17}$$

$$\xi = Cl\ \tanh(Cl) \tag{18}$$

Equations (16)–(18), even though derived for a rectangular geometry, provide a good means of commencing the calculations. The influence of the magnitude of this initial disturbance, specified in terms of the wave amplitude h, on the stability of the interface is also a subject of this investigation.

The numerical experiments were performed for water and glycerol, since the two liquids have significantly different properties. The analytical work of Valha and Kubie [3] neglected the effects of viscosity, but showed the influence of surface tension, whereas the work of

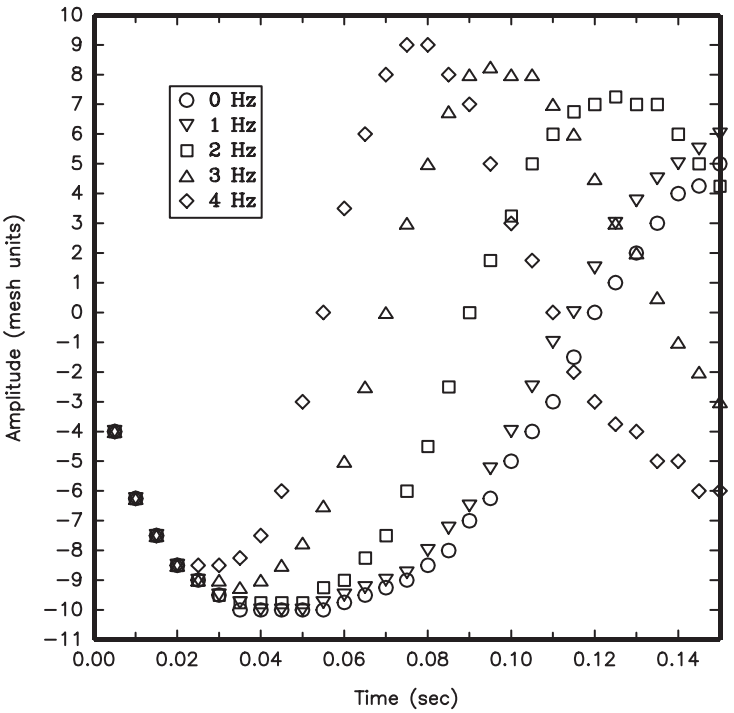

Figure 13. A plot of the wave displacement of glycerol at the axis of symmetry as a function of time ($\sigma = 0.00\ \mathrm{N\ m^{-1}}$, $A = 70\ \mathrm{mm}$, $h = 30\ \mathrm{mm}$).

Kumar and Tuckerman [11], based on a non-linear analysis of the problem, described the influence of viscosity on the frequency of the interfacial wave oscillations. The present numerical analysis allows both surface tension and viscosity effects to be included and thus enables a comparison between computational and analytical results. Three groups of numerical tests were therefore undertaken. In the first group of tests the surface tension phenomena were not taken into account, in the second group of tests the true surface tension values of the two liquids were considered and the CSF model was employed to simulate their effect, and in the third group of tests a higher value of the surface tension was assumed. The amplitude of the forcing oscillations was set at 70 mm for the majority of the tests. This value was chosen because it is approximately in the middle of the range of amplitudes investigated experimentally [3]. However, some tests were also run for an amplitude of the forcing oscillations set at 30 mm.

Figure 6 shows a time sequence of the interfacial position for glycerol but neglecting surface tension. The surface was initially disturbed by a full sinusoidal pulse over the whole surface (shown in Figure 5), where h in Equation (16) was set at 20 mm, and the amplitude and the frequency of the forcing oscillations were set at 70 mm and 3 Hz, respectively. It can be seen that the wave created on the interface does not become unstable in this particular case. The results for the same conditions but including the surface tension phenomenon are shown in Figure 7. The surface tension coefficient of glycerol was taken as $\sigma = 0.030\ \mathrm{N\ m^{-1}}$. Very

little difference can be observed between the marker particle positions in Figures 6 and 7. To investigate fully the significance of surface tension, a set of experiments with the surface tension set at $\sigma = 0.15\ \mathrm{N\ m^{-1}}$ was also run. It should be noted that this value of the surface tension is five times greater than the true value for glycerol. Figure 8 shows the time sequence obtained for the same forcing oscillation conditions as for the cases considered in Figures 6 and 7 but the higher surface tension coefficient. Local surface ripples can now be observed.

Similar numerical experiments were run for water, neglecting the effect of surface tension, with a forcing oscillation amplitude $A = 70\,\mathrm{mm}$ and a frequency $f = 2\,\mathrm{Hz}$. An initial sinusoidal pressure pulse with $h = 2.5\,\mathrm{mm}$ was used. The time sequence of the surface wave propagation is shown in Figure 9. The damping effect of viscosity is now small, since the dynamic viscosity of water is more than 800 times lower than the dynamic viscosity of glycerol, and higher modes of oscillation in the form of local ripples can be observed.

The time histories of the predicted interfacial wave displacements, measured at the axis of symmetry and taken directly from graphs similar to those shown in Figures 6–9, and expressed in terms of mesh units are discussed next. It should be noted that the accuracy of the displacement readings is about 25% of the mesh grid size. The influence of initial pressure pulse disturbance was investigated for values of $h = 5, 10, 20$ and 30 mm and $h = 1, 2.5$ and 5 mm for glycerol and water, respectively. It was found that for both liquids studied and the geometry investigated the surface tension had a negligible effect on the behaviour of the interfacial waves. Figures 10–13 show plots of the wave displacement of glycerol at the axis of symmetry (given in terms of the initial wave amplitude h) as a function of time, with the frequency of the forcing vibrations f as a parameter, and four different values of the initial wave amplitude h, respectively. Figures 14–16 show a similar set of graphs for water.

The experimental results obtained by Valha and Kubie [3] indicate that the critical frequency causing the interfacial wave to grow unstable is, for 70 mm amplitude of the forcing oscillations, 2 Hz for water and 4 Hz for glycerol. In the numerical computations presented in this work exponential wave growth is first observed for glycerol in Figure 11 for a forcing oscillation frequency of 5 Hz and an initial disturbance of $h = 10$ mm. Figures 12 and 13, for the higher values of h, do not indicate that the wave grows unstable for lower forcing frequencies. The numerical results for water are qualitatively different. Figure 14 indicates that for $h = 1$ mm the wave does not grow unstable for the range of frequencies investigated. The results for the initial amplitude of the pulse $h = 2.5$ mm, shown in Figure 15, indicate that the oscillations increase with time for frequencies above about 2 Hz. This is in good agreement with the experimental findings. However, Figure 16 indicates that for $h = 5$ mm the interfacial wave has already grown unstable for a forcing frequency of 1 Hz. Since the analytical solution of the problem was based on the assumption of small oscillations of the interfacial wave, the numerical results indicate that the stability of the interface is dependent not only on the forcing oscillations but also on the initial disturbance applied to the surface.

As discussed above, the analytical results of Valha and Kubie [3] are based on the solution of a Mathieu equation, which can be re-written, assuming that all points on the interface undergo identical oscillations as

$$\frac{\mathrm{d}^2\eta}{\mathrm{d}t^2} + \omega_0^2\left[1 - \frac{k_m A\omega^2\cos(\omega t)}{\omega_0^2}\right]\eta = 0 \tag{19}$$

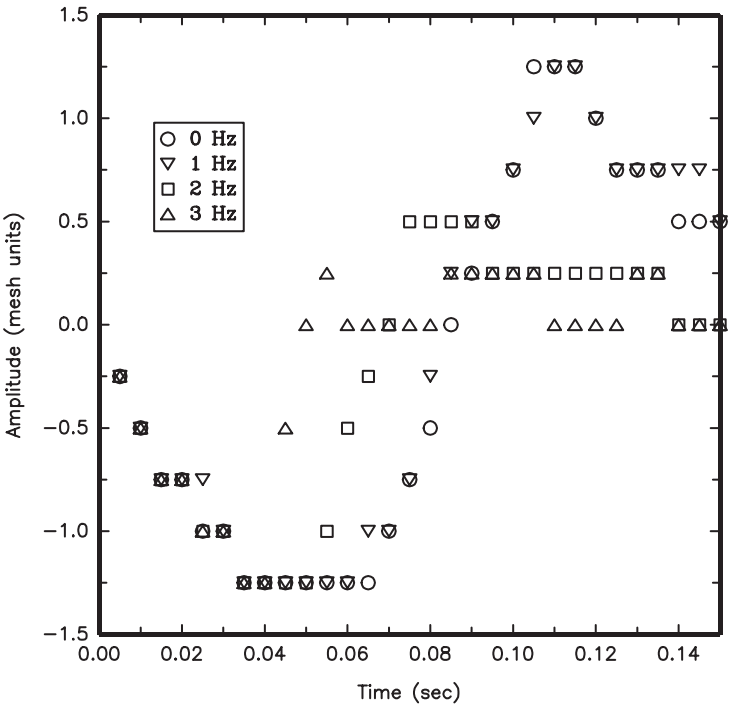

Figure 14. A plot of the wave displacement of water at the axis of symmetry as a function of time ($\sigma = 0.00\,\mathrm{N\,m^{-1}}$, $A = 70\,\mathrm{mm}$, $h = 1\,\mathrm{mm}$).

where

$$\omega_0^2 = \frac{\sigma}{\rho} k_m^3 + g k_m \tag{20}$$

and ω_0 is the undamped angular velocity of oscillations of the interface with no forcing vibrations. The corresponding period of the interfacial wave oscillations can be easily determined from Equation (20). The period of the interfacial oscillations can also be estimated from Figures 10–16. These findings are summarized in Figures 17 and 18 for water and glycerol, respectively.

It can be seen that the magnitude of the initial pulse disturbance has little influence on the half period of oscillation of the interfacial wave. As stated above, Equation (20) gives an expression for the angular velocity of oscillations of the interfacial wave with no forcing vibrations. It should be noted that only the first mode of oscillation is assumed to occur, therefore for the given 69 mm diameter cylinder $k_m = 69.7\,\mathrm{m^{-1}}$. The corresponding analytically derived periodic times (and based on the periodic behaviour) are compared with those obtained numerically (and based on the transient behaviour) in Table I.

As mentioned earlier, and as shown for example in Figure 9, higher modes of oscillation can occur on the liquid surface. This fact is mathematically expressed by the summation over the range of modes of oscillation in the Mathieu equation. However, the Floquet theorem

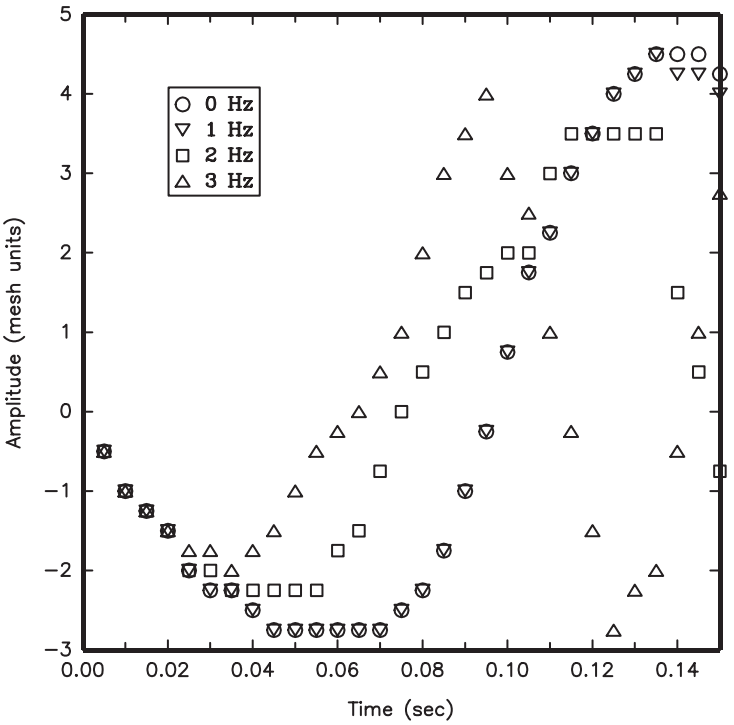

Figure 15. A plot of the wave displacement of water at the axis of symmetry as a function of time ($\sigma = 0.00\ \mathrm{N\ m^{-1}}$, $A = 70\ \mathrm{mm}$, $h = 2.5\ \mathrm{mm}$).

analysis of the governing Mathieu equation presented by Valha and Kubie [3] assumes only a single mode of oscillation. Nevertheless it may be assumed that the value of k_m increases due to the presence of the higher modes and therefore the period of oscillation of the interfacial wave decreases correspondingly. This may provide an explanation of the slight difference between the analytical and CFD results for water. Good agreement between the analytical and computational results is found for glycerol where a single mode of oscillation is present throughout most of the investigated timespan.

Kumar and Tuckerman [11] derived an expression for the angular velocity of interfacial wave oscillations incorporating the effect of liquid viscosity. In their analysis they derived a damping coefficient γ which is based on the rate of dissipation of the total mechanical energy due to viscosity. The expression obtained for the coefficient γ is

$$\gamma = 2k_m^2 v \tag{21}$$

The corrected angular velocity of oscillations, incorporating the effects of viscosity is then given by

$$\omega_{\mathrm{D}}^2 = \omega_0^2 - \gamma^2 \tag{22}$$

where ω_{D} is the angular velocity of the damped oscillations. Equation (22) implies that the period of oscillation of the free surface wave increases with increasing liquid viscosity. This

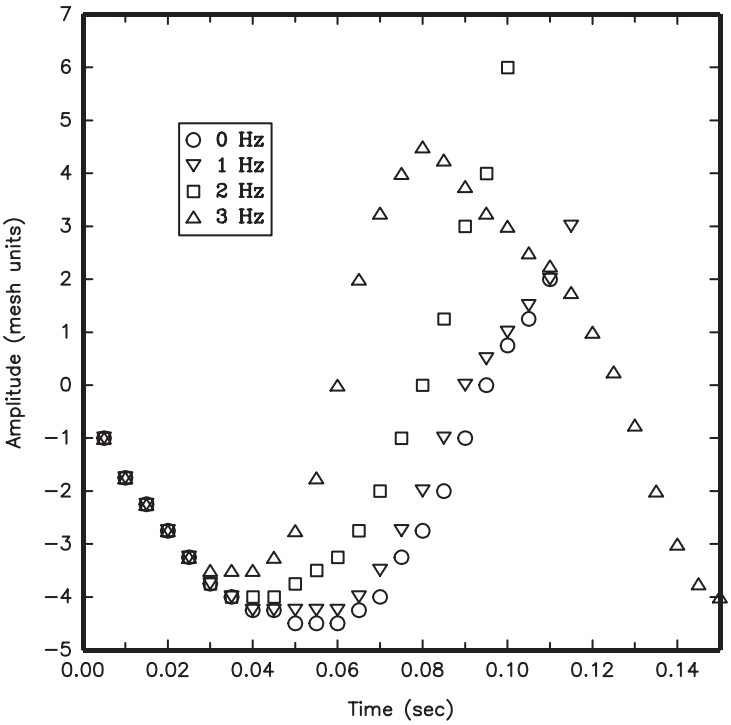

Figure 16. A plot of the wave displacement of water at the axis of symmetry as a function of time ($\sigma = 0.00\,\mathrm{N\,m^{-1}}$, $A = 70\,\mathrm{mm}$, $h = 5\,\mathrm{mm}$).

change is insignificant for water. For glycerol, however, the square of angular velocity of the damped oscillations is about $650\,\mathrm{rad^2\,s^{-2}}$ and the corresponding half period is about 0.12 s. This value is still within the range of the half periods shown in Figure 18 for no forcing vibrations, and there is only a 3% difference between the period of damped and inviscid wave oscillations.

To investigate the influence of the mode of oscillation, numerical experiments were also run for a half sinusoidal initial pressure pulse disturbance. It was found that the wave created on the interface adopted similar oscillatory behaviour to that found in the case when a full sinusoidal initial disturbance was applied on the surface. The corresponding time history of the wave displacement in glycerol is shown in Figure 19. This can be compared with the results presented in Figure 12; it shows that the period of wave oscillation remains unchanged, thus confirming the use of only the first mode of oscillation in the above discussion.

Numerical experiments were also run to investigate the effect of the amplitude of the forcing vibration, including tests for the amplitude $A = 30\,\mathrm{mm}$. Experimental data for glycerol presented by Valha and Kubie [3] show that at this amplitude the critical frequency for the interfacial wave to grow unstable is about 5 Hz. The numerically predicted time history of the wave displacement is shown in Figure 20. It can be observed from Figure 20 that for this particular case the wave created on the interface is clearly unstable for a forcing oscillation frequency of 6 Hz, although it is still stable for 4 Hz. It may be deduced that the point at

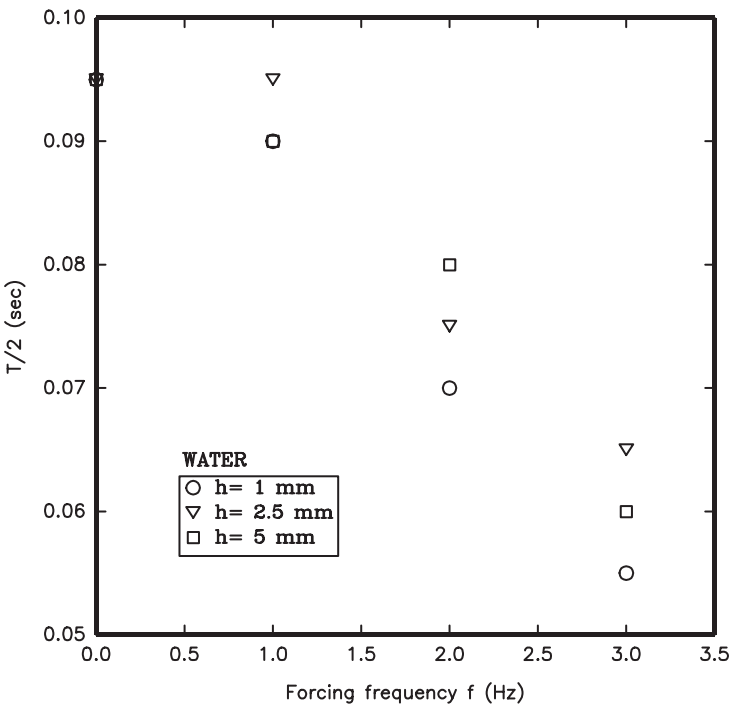

Figure 17. A plot of the periodic time of interfacial oscillations of water as a function of the forcing frequency ($\sigma = 0.00\ \mathrm{N\,m^{-1}}$, $A = 70\ \mathrm{mm}$).

which the sudden instability occurs lies within the range of these two values, which is in good agreement with the experimental finding.

A comparison of the periods of oscillation of the interfacial waves for forcing vibration amplitudes of 30 and 70 mm, as shown in Figures 20 and 12, respectively, shows that at any given forcing frequency the oscillation period is shorter for the higher amplitude case, particularly for the higher forcing frequencies. This agrees with the analytical results.

Figures 10–16, 19 and 20 indicate that the frequency of oscillation of the interfacial wave increases with increasing forcing frequency. This is, once again, supported by the analytical solutions which show that the frequency of oscillations of the interfacial wave is determined uniquely by the frequency of the forcing vibrations. The wave can oscillate with angular velocities equal to the multiples of half of the angular velocity of the forcing vibrations.

4. CONCLUSIONS

A computational analysis has been carried out to examine the behaviour, especially the stability, of a gas liquid interface in a vertical cylindrical vessel subjected to a sinusoidal vertical motion. Water and glycerol were the liquids considered. The work follows the earlier published analytical solutions of the problem.

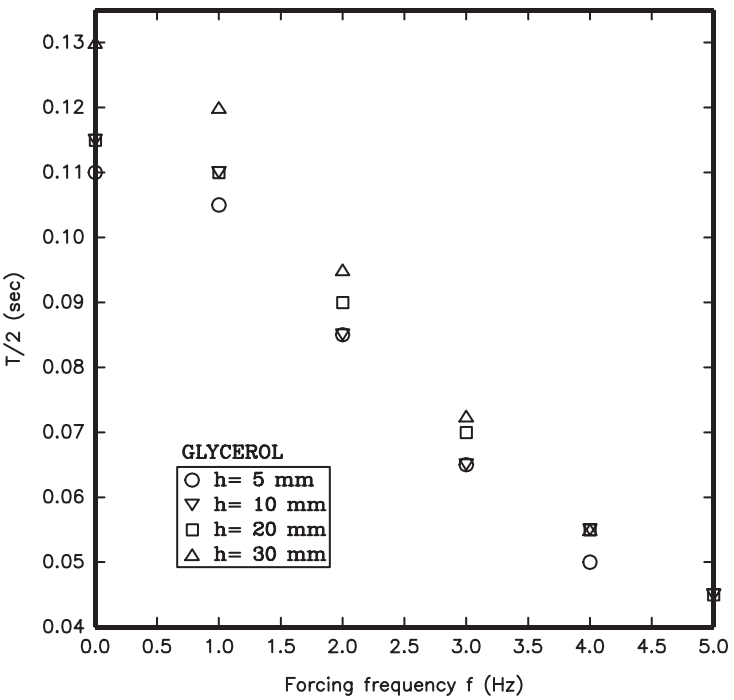

Figure 18. A plot of the periodic time of interfacial oscillations of glycerol as a function of the forcing frequency ($\sigma = 0.00\ \mathrm{N\,m^{-1}}$, $A = 70\ \mathrm{mm}$).

The computational method used is based on a SMAC, which uses the continuum surface force model for the incorporation of the surface tension. It has been found that the surface tension has very little effect on the period and amplitude of oscillation of the interfacial wave. However, small local ripples caused by surface tension effects do occur. The computations indicate that higher modes of oscillation are established on the stability boundary.

It has also been found that the magnitude of the initial sinusoidal pressure disturbance imposed on the interface does not have any significant effect on the period of oscillation of the interfacial wave, but that it does influence its amplitude. The stability of the interfacial wave has been found to depend on the initial pressure pulse disturbance, and exponential growth of the interfacial wave has been observed in some cases. The period of wave oscillation determined computationally for a cylinder without forcing oscillations agrees well with the analytical findings. The agreement is particularly good for high viscosity liquids such as glycerol.

Numerical experiments have been also performed for a half sinusoidal initial pressure disturbance on the surface to investigate the influence of the mode of oscillation. It has been found that the wave created on the interface establishes an oscillatory behaviour similar to that found in the case of a full sinusoidal disturbance, thus confirming that only a single dominant mode of oscillation occurs.

Finally, the influence of the amplitude of the forcing oscillation has also been investigated. The computational findings suggest that for the higher values of the amplitude and a particular

Table I. Comparison of the analytical and computational results for the period of oscillations of the interfacial waves obtained with no forcing vibrations.

	Analytical results		Computational results
	ω_0 (rad s^{-1})	T_0 (s)	T_0 (s)
Water	26.6	0.236	0.19
Glycerol	26.3	0.238	0.24*

*Average value over the range of h investigated.

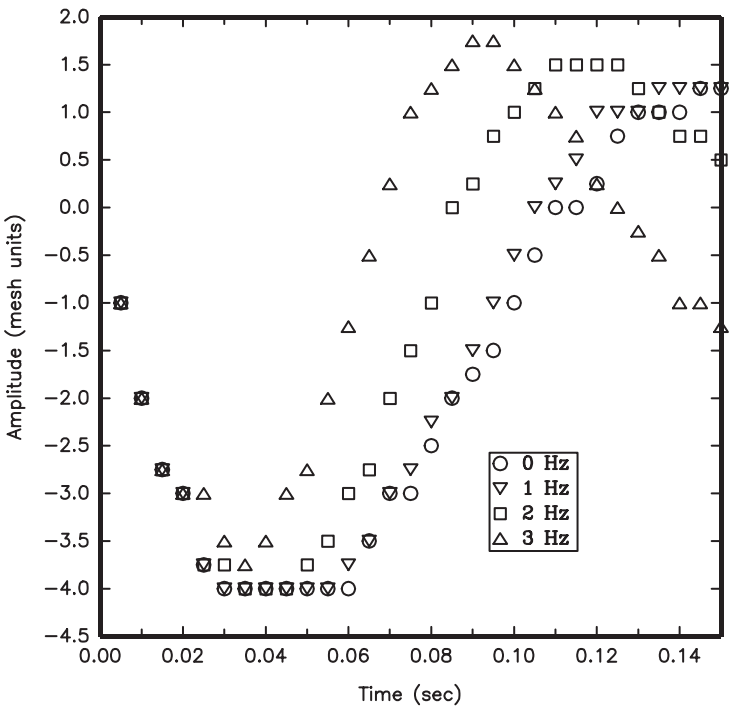

Figure 19. Effect of half sinusoidal initial disturbance on the wave displacement of glycerol at the axis of symmetry as a function of time ($\sigma = 0.00\,\mathrm{N\,m^{-1}}$, $A = 70\,\mathrm{mm}$, $h = 20\,\mathrm{mm}$).

frequency, the oscillation period decreases, which agrees well with the analytical results. The computations have also shown that with the increasing frequency of the forcing vibration the frequency of oscillations of the interfacial wave also increases. This is, once again, supported by the analytical solutions.

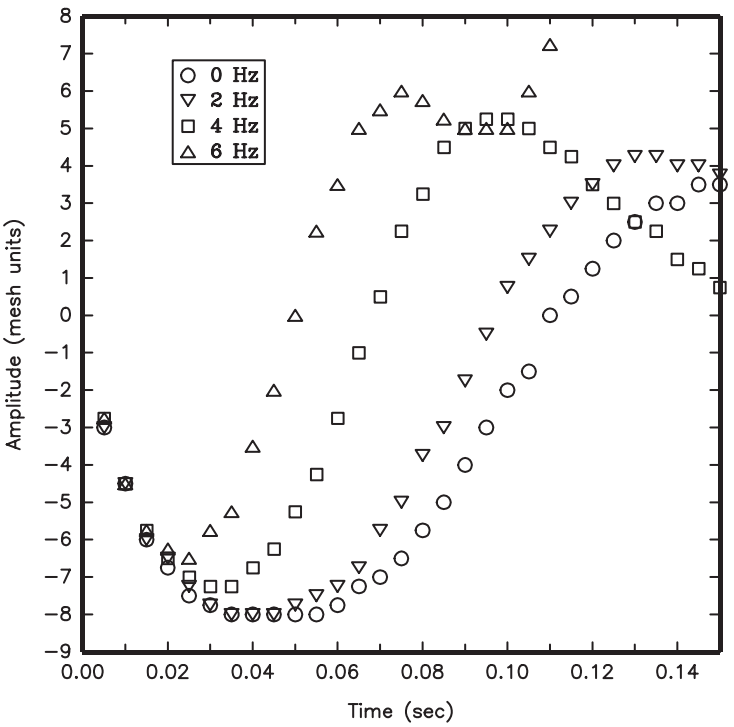

Figure 20. Effect of the amplitude of the forcing vibration on the wave displacement of glycerol at the axis of symmetry as a function of time ($\sigma = 0.00\,\mathrm{N\,m^{-1}}$, $A = 30\,\mathrm{mm}$, $h = 20\,\mathrm{mm}$).

NOMENCLATURE

a	oscillatory acceleration, $\mathrm{m\,s^{-2}}$
A	amplitude of oscillatory motion, m
B	parameter given by Equation (16), $\mathrm{m^2\,s^{-1}}$
C	parameter given by Equation (17), $\mathrm{m^{-1}}$
D	continuity function, $\mathrm{s^{-1}}$
f	forcing frequency, Hz
F	volume of fluid function
F_b	body force source due to surface tension, $\mathrm{m\,s^{-2}}$
F_{sv}	continuum surface force, $\mathrm{N\,m^{-3}}$
g	gravitational acceleration, $\mathrm{m\,s^{-2}}$
h	amplitude of the initial disturbance, m
k	wave number, $\mathrm{m^{-1}}$
l	height of liquid column, m
L	height of the cylinder, m
n	direction vector
r	horizontal co-ordinate, m
R	radius of the cylinder, m

t time, s
T period of oscillations of interfacial waves, s
T_0 period of oscillations of interfacial waves with no forcing vibrations, s
u velocity in r direction, $m\,s^{-1}$
v velocity in z direction, $m\,s^{-1}$
X parameter
z vertical co-ordinate, m

Greek letters

Φ true pressure normalized to unity density, $m^2\,s^{-2}$
γ damping coefficient, s^{-1}
η interface displacement measured from equilibrium position, m
κ curvature of the interface, m^{-1}
ν kinematic viscosity, $m^2\,s^{-1}$
θ arbitrary pressure field, Pa
ρ density, $kg\,m^{-3}$
σ surface tension, $N\,m^{-1}$
ω angular velocity of the imposed oscillatory motion, $rad\,s^{-1}$
ω_D damped angular velocity of oscillations of the interface with no forcing vibrations, $rad\,s^{-1}$
ω_0 undamped angular velocity of oscillations of the interface with no forcing vibrations, $rad\,s^{-1}$
Ω vorticity, s^{-1}
ξ parameter given by Equation (18)

Subscripts and superscripts

i, j mesh positions
m order of mode oscillation
r horizontal direction
z vertical direction
α co-ordinate exponent
$\hat{}$ unit vector
$\rightarrow$ vector

REFERENCES

1. Faraday M. On the forms and states of fluids on vibrating elastic surfaces. *Philosophical Transactions of the Royal Society of London* 1831; **52**:319–340.
2. Rayleigh Lord. On the crispations of fluid resting upon a vibrating support. *Philosophical Magazine* 1883; **16**: 50–58.
3. Valha J, Kubie J. Stability of a gas–liquid interface in a periodic vertical motion. *Chemical Engineering Science* 1996; **51**:4997–5006.
4. Valha J. Interfacial instability and spray heat transfer problems of two phase flow. *Ph.D. Thesis*, Energy Technology Centre, Middlesex University, London, 1996.
5. Welch JE, Harlow FH, Shannon JP, Daly BJ. The MAC method—a computing technique for solving viscous, incompressible, transient fluid-flow problems involving free surfaces. *Los Alamos Scientific Laboratory Report LA*-3425, 1965.
6. Amsden AA, Harlow FH. The SMAC method: a numerical technique for calculating incompressible fluid flows. *Los Alamos Scientific Laboratory Report LA*-4370, 1970.

7. Kothe DB, Mjolsness RC, Torrey MD. Ripple: a computer program for incompressible flows with free surfaces. *Los Alamos National Laboratory Report LA*-12007-MS, 1991.
8. Hirt CW, Nichols BD. Volume of fluid (VOF) method for the dynamics of free boundaries. *Journal of Composite Physics* 1981; **39**:201–228.
9. Drazin P, Reid W. *Hydrodynamic Stability*. Cambridge Monographs on Mechanics and Applied Mathematics, Cambridge University Press: Cambridge, 1981.
10. Brackbill JU, Kothe DB, Zemach C. A continuum method for modelling surface tension. *Journal of Composite Physics*, 1992; **100**:335–354.
11. Kumar K, Tuckerman LS. Parametric instability of the interface between two fluids. *Journal of Fluid Mechanics* 1994; **279**:49–68.

